

# Spin interfaces and crossing probabilities of spin clusters in parafermionic models

---

Yoshiki Fukusumi<sup>1</sup>, Marco Picco<sup>2</sup>, Raoul Santachiara<sup>3</sup>

<sup>1</sup> *Department of Physics, Faculty of Science, University of Zagreb, HR-10000 Zagreb, Croatia*

<sup>2</sup> *Sorbonne Université, CNRS UMR 7589, Laboratoire de Physique Théorique et Hautes Energies, 4 Place Jussieu, 75252 Paris Cedex 05, France*

<sup>3</sup> *Université Paris-Saclay, CNRS, LPTMS, 91405, Orsay, France*

**ABSTRACT:** We consider fractal curves in two-dimensional  $Z_N$  spin lattice models. These are  $N$  states spin models that undergo a continuous ferromagnetic-paramagnetic phase transition described by the  $Z_N$  parafermionic field theory. The main motivation here is to investigate the correspondence between Schramm-Loewner evolutions (SLE) and conformal field theories with extended conformal algebras (ECFT). By using Monte-Carlo simulation, we compute the fractal dimension of different spin interfaces for the  $N = 3$  and  $N = 4$  spin models that correspond respectively to the  $Q = 3$  Potts model and to the Ashkin-Teller model at the Fateev-Zamolodchikov point. These numerical measures, that improve and complete the ones presented in the previous works [1, 2], are shown to be consistent with SLE/ECFT predictions. We consider then the crossing probability of spin clusters in a rectangular domain. Using a multiple SLE approach, we provide crossing probability formulas for  $Z_N$  parafermionic theories. The parafermionic conformal blocks that enter the crossing probability formula are computed by solving a Knizhnik-Zamolodchikov system of rank 3. In the  $Q = 3$  Potts model case ( $N = 3$ ), where the parafermionic blocks coincide with the Virasoro ones, we rederive the crossing formula found in [3] that is in good agreement with our measures. For  $N \geq 4$  where the crossing probability satisfies a third order differential equation instead of a second order one, our formulas are new. The theoretical predictions are compared to Monte-Carlo measures taken at  $N = 4$  and a fair agreement is found.

---

## Contents

<b>1</b>	<b>Introduction</b>	<b>1</b>
<b>2</b>	<b>The <math>Z_N</math> spin interfaces and their fractal dimension</b>	<b>2</b>
2.1	The $Z_3$ and $Z_4$ spin models	2
2.2	Spin interfaces in the $Q = 3$ Potts model	4
2.3	Spin interfaces in the $Z_4$ model	5
<b>3</b>	<b><math>Z_N</math> crossing probability</b>	<b>8</b>
3.1	Theoretical predictions	8
3.2	Measurements	11
3.2.1	(1 23) Potts spin interface	12
3.2.2	$Z_4$ spin model	13
<b>4</b>	<b>Conclusion</b>	<b>15</b>
<b>A</b>	<b><math>Z_N</math> parafermionic theory</b>	<b>16</b>
A.1	Ising case, $N = 2$	17
<b>B</b>	<b>Computation of <math>G_N(x)</math> for <math>N \geq 4</math></b>	<b>18</b>
B.1	$SU(2)_N$ conformal blocks and Khzniznik-Zamolodchikov equation	19
B.1.1	Coulomb gas representation of the rank 3 KZ system	19
B.1.2	Solution of the rank 3 KZ by the Frobenius method	21

---

## 1 Introduction

The study of the fractal objects appearing in critical phenomena, and the role of conformal invariance in describing their behavior, represents one of the most significant problems of current statistical and mathematical physics. Important insights into the nature of conformal fractals have been provided recently by studying the geometric [4, 5] and topological [6–8] properties of percolation clusters. These results have been obtained using a conformal bootstrap approach that provides a new and powerful angle of attack to these problems. Here we consider different fractal objects: instead of fractal domains, we study fractal curves defined as the boundaries of spin clusters. A very well known method to construct conformal fractal curves is the Schramm-Loewner Evolution (SLE)[9]. The SLE correspondence to Conformal Field Theory (CFT) enables us to analyze 2D statistical models in a wide variety of geometries [10] and should shed a unified understanding of boundary critical phenomena and stochastic processes. One of the main motivation behind this work is to investigate the correspondence between the SLE and CFT with extended infinite symmetries (ECFTs) that adds to the conformal one [11, 12]. An important example of ECFTs are the  $Z_N$  parafermionic theories that describe the critical point of  $Z_N$

invariant lattice spin models [13]. These models include the Ising ( $N = 2$ ), the 3-states spin Potts model ( $N = 3$ ) and the Ashkin-Teller model at the Fateev-Zamolodchikov point ( $N = 4$ ). The latter two models, defined in (2.1) and in (2.2) are the object of the Monte-Carlo simulations presented here.

In [14, 15] the SLE/ECFT correspondence was used to predict the fractal dimension for spin interfaces in  $Z_N$  spin models. The SLE approach to the entire critical line of the Ashkin-Teller model, which includes the  $Z_4$  spin model, has been further discussed in [16, 17]. In [18] multiple SLE processes in these theories were also considered. By Monte-Carlo simulations, we measure first the fractal dimension of different spin interfaces, showing that certain spin interfaces have a fractal dimension that is consistent with the predicted values. Note that these measures improve and complete the ones presented in previous papers [1, 2].

We study then the crossing probability of  $Z_N$  spin clusters by using the multiple SLE approach of [18]. The analytical predictions are then compared to Monte-Carlo measures, taken for the  $Z_3$  and  $Z_4$  spin lattice model on rectangular domain. The case  $N \geq 4$  is particularly interesting to further test the SLE/ECFT correspondence. Indeed, the role of the extended symmetry becomes important and the formulas deviate from the ones concerning CFTs based on Virasoro algebras only. Moreover, at the level of the  $Z_N$  spin lattice models, for  $N \geq 4$  the identification of all the boundary conformal states in terms of spin configuration is not known. In the simulations, we test different boundary conditions that generate a single spin interfaces and we select the ones that are better described by the fractal dimension predicted by the SLE/ECFT correspondence.

In section 2, we define the models and the spin interfaces we simulate. We present new numerical results for the fractal dimension of spin interfaces for the  $Q = 3$  Potts model and the  $Z_4$  spin model. In section 3 we consider the crossing probability of  $Z_N$  spin cluster in rectangular domains. We compare analytical prediction to numerical data for the  $Q = 3$  Potts model and the  $Z_4$  spin model. The details of the computation of the parafermionic blocks entering the  $Z_N$  crossing formula are given in the Appendixes. We summarise the results in the Conclusion.

## 2 The $Z_N$ spin interfaces and their fractal dimension

In this paper, we will present accurate measurements of fractal dimensions for spin interfaces and crossing probabilities for the  $Z_3$  and  $Z_4$  parafermionic spin models on square lattice of rectangular shape.

### 2.1 The $Z_3$ and $Z_4$ spin models

The  $Z_3$  parafermionic spin model, that coincides with the  $Q = 3$  spin Potts model, is defined by the Hamiltonian:

$$H_{Z_3} = - \sum_{\langle ij \rangle} K \delta_{S_i S_j}, \quad (2.1)$$

where  $S_i$  is the spin variable taking values  $S_i = 1, 2, 3$  and the sum is restricted to the neighbouring sites  $\langle ij \rangle$ . The ferromagnetic-paramagnetic transition is located, for the square lattice, at  $K_c = \log(1 + \sqrt{3})$  and it is described by the  $Z_3$  parafermionic theory

that has central charge  $c = 4/5$ . The thermal and magnetic sector of this theory coincides with the one of the Virasoro (non-diagonal) minimal model of the  $D-$  series [4].

The  $Z_4$  parafermionic spin model coincides with the Ashkin-Teller (AT) model at a particular values of the couplings. This latter model [19] can be defined in terms of two coupled Ising models: on each site  $i$  of a square lattice one associates a pair of spins, denoted by  $\sigma_i$  and  $\tau_i$ , which take two values, say up(+) and down(-). The Hamiltonian is defined by

$$H_{Z_4} = - \sum_{\langle ij \rangle} K(\sigma_i \sigma_j + \tau_i \tau_j) + K_4 \sigma_i \sigma_j \tau_i \tau_j . \quad (2.2)$$

The two parameters,  $K$  and  $K_4$ , correspond respectively to the usual Ising spin interaction and to the 4-spins coupling between two Ising models. Using the map:

$$\begin{aligned} S_i = 1 &\rightarrow \sigma_i = +, \tau_i = + ; & S_i = 2 &\rightarrow \sigma_i = +, \tau_i = - \\ S_i = 3 &\rightarrow \sigma_i = -, \tau_i = - ; & S_i = 4 &\rightarrow \sigma_i = -, \tau_i = + ; \end{aligned}$$

one can rewrite the AT model in terms of a one layer of spins  $S_i$  that take four values and interact via next-neighbours interactions. The AT model, that on a square lattice is equivalent to the staggered six vertex model [20, 21], presents a rich phase diagram [20–22]. There exists a critical line which is defined by the self-dual condition

$$\sinh 2K = \exp(-2K_4) \quad (2.3)$$

and terminates at  $\coth 2K_2 = 2$ . The point on the critical line defined by:

$$x_1^{\text{FZ}} = \frac{\sin(\frac{\pi}{16})}{\sin(\frac{3\pi}{16})} ; x_2^{\text{FZ}} = x_1 \frac{\sin(\frac{5\pi}{16})}{\sin(\frac{7\pi}{16})} , \quad (2.4)$$

where  $x_1$  and  $x_2$  are related to  $K$  and  $K_4$  :

$$\exp(4K) = \frac{1 + 2x_1 + x_2}{1 - 2x_1 + x_2} ; \quad \exp(2K + 2K_4) = \frac{1 + 2x_1 + x_2}{1 - x_2} . \quad (2.5)$$

is called the Fateev-Zamolodchikov point. At this point the model has been shown to admit special integrable properties [23, 24] and to be described, in the continuum limit, by the  $Z_4$  parafermionic theory.

One can define different types of interfaces in these two models according to the colors of spins they separate. For instance, in the  $Q = 3$  Potts model, the interface (1|23) separates the spin of color 1 from the spins of colors 2 or 3. Or, in the  $Z_4$  spin model, the interface (12|34) separates the spin of color 1 or 2 to the spins of color 3 or 4. These interfaces are defined in the bulk. The same notation is used for the spin boundary conditions that generate a single boundary interface. We consider the following boundary conditions. For the  $Q = 3$  Potts model:

- (1|23): this corresponds to fix  $S_i = 1$  on the top and bottom boundaries (of length  $L_x$ ) while the spins on the two other boundaries can take all values different from 1

Note that, in the case of Virasoro minimal models, crossing probability formulas for general polygonal domains and general central charges, have been given in [3]. These formulas include as a special case the formula (3.9) derived here. For the  $Z_4$  model, natural choices of boundary conditions are:

- (1|234): from (2.3), this corresponds to fix  $S_i = 1$  on the top and bottom boundaries (of length  $L_x$ ) while the spins on the two other boundaries can take all values different from 1, i.e.  $S_i \in (2, 3, 4)$ . In terms of the Ising degrees of freedom, this is equivalent to set  $\sigma_i = +$  and  $\tau_i = +$  on the top and bottom boundaries and any other choice on the two other boundaries.
- (12|34) : on the top and bottom boundaries,  $S_i \in (1, 2)$  on the left and right boundaries  $S_i \in (3, 4)$ . This corresponds to impose  $\sigma_i = +$  on the top and bottom boundaries while  $\sigma_i = -$  on the other two boundaries. The same conditions have been considered in [16] for the entire critical line of the AT model.
- (13|24): on the top and bottom boundaries  $S_i \in (1, 3)$ , on the left and right boundaries  $S_i \in (2, 4)$ . This corresponds to  $\sigma_i = +, \tau_i = +$  or  $\sigma_i = -, \tau_i = -$  on the top and bottom boundaries and  $\sigma_i = +, \tau_i = -$  or  $\sigma_i = -, \tau_i = +$  on the two other boundaries.

Due to the symmetry of the system, it is easy to see that these are the only conditions that can be considered. There exists also conditions like (1|2) but then there can be no connecting cluster between opposite boundaries. We will not consider these cases here.

## 2.2 Spin interfaces in the $Q = 3$ Potts model

The boundary conditions (1|23) were considered in [25]. For this model, the authors predicted the fractal dimension of the interface to be  $d_f = 1 + (10/3)/8$  and indeed found this result when considering fluctuating boundary conditions with a single interface. They also consider the case with fixed boundary conditions (1|2). On one part of the boundary, the spins are fixed to the type  $S_i = 1$  while the spins on the remaining boundary are fixed to the value  $S_i = 2$ . The generated interface can then be separated in two parts : a first one, of length  $l_{\text{composite}}$ , separates spins of color  $S = 1$  connected to the boundary with  $S = 1$  and spins of color  $S = 2$  connected to the boundary  $S = 2$  and is called the composite part; the remaining part of the interface, of length  $l_{\text{split}}$ , which touch spins of color  $S = 3$  or isolated clusters is called the split part. The fractal dimensions are not the same for the two parts. Gamsa and Cardy obtained  $d_f \simeq 1.0$  for the composite part and  $d_f \simeq 1.6$  for the split part [25]. More accurate results [26] show that in fact this is not the case. By considering larger sizes and more statistics, it can be seen that the split interface is composed of two parts.

In Fig. 1 we show effective fractal dimensions as a function of  $L$  in a fit with data between the size  $L$  and the maximum size  $L_m = 5120$ . In this figure, we show various quantities. First the fractal dimension for the total interface  $l_{\text{composite}} + l_{\text{split}} \simeq L^{d_f}$ . It converges very nicely towards the expected value  $d_f = 1 + (10/3)/8$ . Next, the fractal dimension for the split interface which has an effective exponent decreasing very slowly. At intermediate sizes, the value is close to the one obtained by Gamsa and Cardy but for the largest sizes that we simulate, it goes to smaller values. We also show that the fractal dimension for the composite interface which decreases slowly down to  $\simeq 0.98$ . Again, at intermediate sizes, it is compatible with the finding of Gamsa and Cardy. Next, for the split interface, we show the result of a fit with two exponents as in eq. (2.8). These two

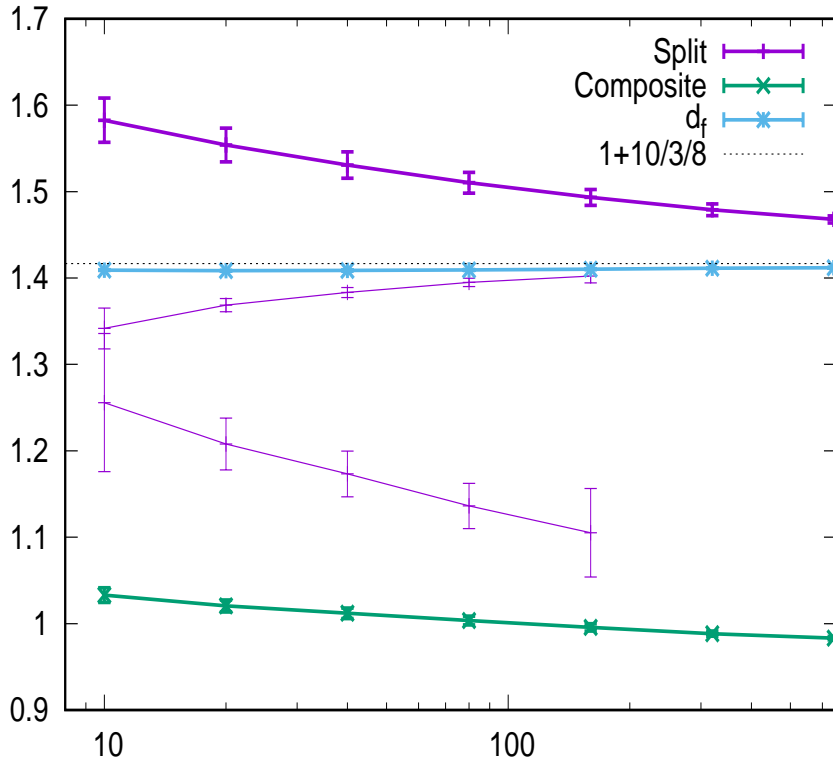


**Figure 1.** Effective fractal dimensions for the  $Q = 3$  state Potts model as a function of the smallest size  $L$  in the fit. See the text for details.

effective exponents are shown with thin lines with the same color. We observe that one of the exponents goes towards the fractal dimension of the fluctuating boundary conditions  $d_f = 1 + (10/3)/8$ . The second fractal dimension seems to converge towards the value of the fractal dimension of the composite interface. This last measurement is plagued by large error bars, as can be expected since it is a subdominant exponent.

Then, for the  $Q = 3$  Potts model, the split interface is just the trivial sum (or more precisely difference) of two scaling interfaces.

### 2.3 Spin interfaces in the $Z_4$ model

We will show in the following that analogous results are obtained for the  $Z_4$  model.

In [1, 2, 27], the fractal dimension of the interfaces based on boundary conditions (1|234), (12|34) and (13|24) were considered. In these numerical measurements, even for the largest systems considered, we observed important finite size corrections. Then it was not possible to determine with a great precision the fractal dimension. In these simulations, the main limitation was due to the fact that we considered lattices with fixed boundary conditions. This has the consequence to slow down the Monte Carlo updates and then limit the precision one can get. We present here some alternative way for performing similar measurements with some new results.

Another method is to determine the fractal dimensions of bulk interfaces. This was already done in [1] where we considered the fractal dimensions of finite clusters. In that case, one needs to compare the average volume of the clusters with the average length of

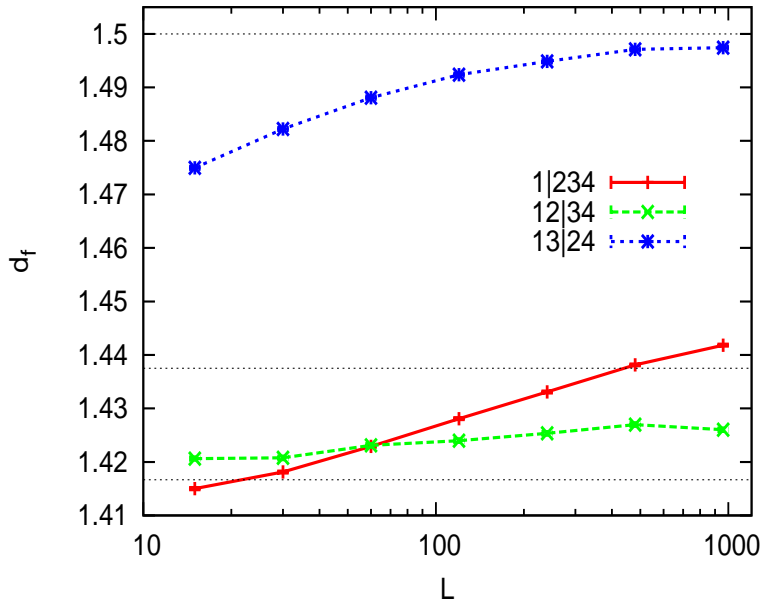


**Figure 2.** Fractal dimension  $d_f$  as a function of  $L$  for the conditions (1|234), (12|34) and (13|24) for the  $\mathcal{Z}_4$  parafermion model. The dashed lines correspond to  $1 + 10/24$ ,  $1 + 7/16$  and  $3/2$ .

the interface surrounding them, which makes the measurement indirect. In this paper, we propose a different way of doing this measurement. We will simulate systems with periodic boundary conditions and for each independent configurations, we will consider the largest cluster. More precisely, we will compute the largest cluster  $\mathcal{C}_1$  containing only one value of the spin  $S_i$ , the largest cluster  $\mathcal{C}_{12}$  containing only states with  $S_i = 1$  or 2 and the largest cluster  $\mathcal{C}_{13}$  containing only states with  $S_i = 1$  or 3. Since we are at a critical point, the probability that a cluster of any type percolates is finite. If one considers a lattice with periodic boundary conditions, then there is a finite probability that this percolating cluster is wrapping through the lattice such that the borders of the cluster correspond to two interfaces. In this new approach, we measure the average length of these interfaces and we use them to define the fractal dimension via the relation

$$l \simeq L^{d_f} \quad (2.6)$$

where  $l$  the length of the interface and  $L$  the lattice size. The advantage of this method is that the auto-correlation time is much smaller than in the case with fixed boundary conditions. For example, for  $L = 640$ , the auto-correlation time is determined to be  $\tau = 356$  while it is  $\tau \simeq 25000$  for the case with an interface generate by fixed boundary conditions (1|234). This allows us to better compute  $d_f$  for the various cases, achieving a much better accuracy. In Fig. 2, we show the effective fractal dimension for the  $\mathcal{Z}_4$  parafermion model obtained for the various cases using the following formula :

$$d_f^{eff}(1.5L) = \frac{\log(l(2L)/l(L))}{\log 2}. \quad (2.7)$$

Notice that in Figure 2, error bars are very small. This was made possible by accumulating

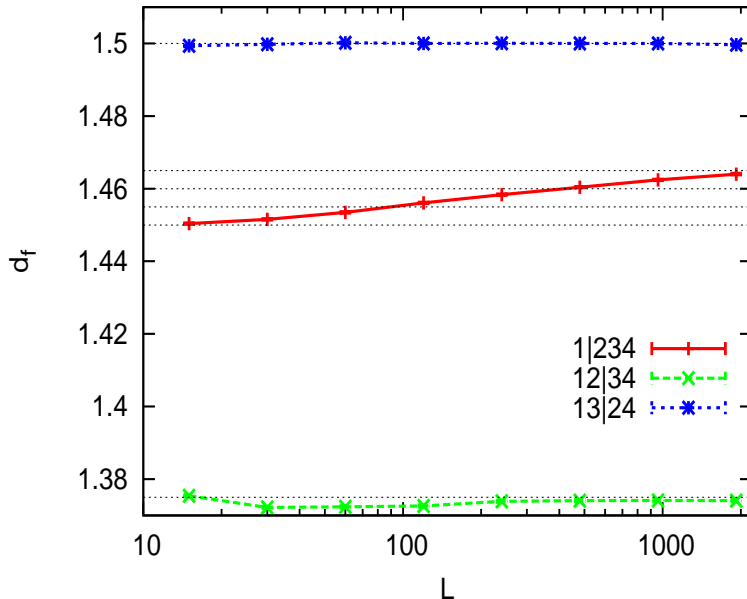


**Figure 3.** Fractal dimension  $d_f$  as a function of  $L$  for the conditions (1|234), (12|34) and (13|24) for two decoupled Ising models (also known as XOR model). The dashed lines correspond to  $1 + 3/8$ ,  $3/2$  on the right. We also add some dashed lines at intermediate values as a guide to the eye.

a lot of data, namely  $10^8$  independent configurations. The total computing time for the largest run ( $L = 1280$  of the  $\mathcal{Z}_4$  parafermion model) corresponds to 100 years of run on a single processor.

For the condition (13|24) we observe a nice convergence towards the value  $3/2$ , consistently with what was already obtained in previous works [2, 27]. For the condition (12|34), we observe that, even if the finite size corrections are still visible, it seems reasonable to expect that the large size limit will be in the range  $1.42 - 1.44$ . This is compatible with the prediction  $1 + 7/16$ , discussed previously. For the condition (1|234) we observe that the effective fractal dimension is constantly increasing with no apparent saturation. It is difficult to predict the asymptotic limit, but one can expect that it will saturate towards  $1.5$ . Similar measurements were also done for the decoupled point of the Ashkin-Teller line and a similar behavior is observed, see Fig. 3. For that point, the fractal dimension for the condition (1|234) does also not converge and moves slowly towards the value  $3/2$ . The fractal dimensions for the two other conditions converge nicely to the expected dimensions, respectively to  $d_f = 1 + 3/8$  and  $d_f = 3/2$ .

A simple scenario to interpret the above numerical observation is that the condition (1|234) corresponds to a mixing of two conformal boundary conditions. The dominant one would have a dimension  $3/4$  and the second a smaller dimension with a value close to the condition (12|34). As a check, we replaced the relation (2.6) by

$$l \simeq L^{d_{f_1}} + L^{d_{f_2}} . \quad (2.8)$$

In the case of two decoupled Ising model, we obtain a good fit of the length of the interface  $l$  for the boundary condition (1|234) with the fixed value  $d_{f_2} = 1.5$  and with  $d_{f_1} \simeq 1.38$ ,



The 0,  $x$  and 1 are the points where the boundary conditions change and where three simple (1|23) interfaces are generated. The partition function  $Z$  can be seen as a sum of two partition functions:

$$Z(x) = Z_I(x) + Z_{II}(x), \quad (3.2)$$

where  $Z_I$  ( $Z_{II}$ ) is the partition function of the configurations where the interface generating at 1 (at 0) collides with the point at infinity. The boundary changing condition (b.c.c.) field associate to (1|23) is the field  $\varepsilon$  with dimension  $\Delta_\varepsilon = \frac{2}{5}$ . The  $Z_I$  and  $Z_{II}$  are related to the conformal blocks that contain four  $\varepsilon$  fields:

$$G_3(x) = \langle \varepsilon(0)\varepsilon(x)\varepsilon(1)\varepsilon(\infty) \rangle_{Z_3}. \quad (3.3)$$

The parafermionic block  $G_3(x)$  coincides with the conformal block with four Virasoro fields, with the same dimension, and degenerate at level two. We refer the reader to the Appendix of [14] for a detailed proof of this. In Appendix A.1 we show an analogous result for the Ising model ( $N = 2$ ).  $G_3(x)$  satisfies a second order differential equation of hypergeometric type and it can in general be expanded on the two solutions:

$$\begin{aligned} G_3^{(1)}(x) &= x^{-\frac{4}{5}}(1-x)^{\frac{3}{5}} {}_2F_1\left(\frac{6}{5}, -\frac{1}{5}, -\frac{2}{5}; x\right), \\ G_3^{(2)} &= x^{\frac{3}{5}}(1-x)^{\frac{3}{5}} {}_2F_1\left(\frac{6}{5}, \frac{13}{5}, \frac{12}{5}; x\right). \end{aligned} \quad (3.4)$$

The small  $x$  behavior  $G_3^{(i)}(x) \sim x^{\Delta^{(i)} - \frac{4}{5}}(x \ll 1)$ , associates the two solutions respectively to the identity channel  $\Delta^{(1)} = 0$  and to the  $\Delta^{(2)} = \frac{7}{5}$  channel. In order to find how  $Z_I$  and  $Z_{II}$  are expressed in terms of the  $G_3^{(i)}$ , we study the behavior of  $Z_{II}(x)$  in the limit for  $x \rightarrow 0$ . In this limit, the  $Z_{II}$  is described by a 2SLE $_\kappa$  process, with  $\kappa = \frac{10}{3}$ . This is a Bessel process with fractal dimension [28]:

$$d_f = 2 + 2(\Delta^{(i)} - 2\Delta_\varepsilon) - \frac{4}{\kappa} = 2 + 2\Delta^{(i)} - \frac{7}{5}. \quad (3.5)$$

If we impose the non-recurrent condition for the Bessel process, we have

$$d_f > 2, \quad (3.6)$$

which implies:

$$Z_{II}(x) \propto G_3^{(2)}(x). \quad (3.7)$$

One observes also that, as  $Z_{II}(1-x)$  corresponds to  $Z_I(x)$  with the boundary conditions 1 and 23 interchanged, one expects  $Z_I(x) = \beta Z_{II}(1-x)$ , where  $\beta$  is some constant. The fact that  $\beta \neq 1$  originates from the fact that the condition 1 and 23 are not symmetric. The constant  $\beta$  can be determined by imposing that the total partition function  $Z(x) = Z_I(x) + Z_{II}(x) \sim x^{-\frac{4}{5}}z(x)$ , where  $z(x)$  is polynomial in  $x$ . Using the monodromy properties of the hypergeometric function, one finds:

$$\beta = -\frac{\Gamma(-\frac{1}{5})\Gamma(\frac{6}{5})}{\Gamma(-\frac{7}{5})\Gamma(\frac{12}{5})} \sim 1.61803 \quad (3.8)$$



associated to the three possible fields appearing in the fusion  $\varepsilon \times \varepsilon$ , see (B.14) and (B.26). The first terms in the small  $x$  expansions of the  $G_4^{(i)}(x)$  are given in (B.37). The  $Z_I$  and  $Z_{II}$  can therefore be expanded on the  $G_N^{(i)}$  basis, where:

$$G_N^{(i)}(x) \sim \langle \varepsilon(0)\varepsilon(x)\phi^{(i)}(\infty) \rangle \sim x^{-2\Delta_\varepsilon + \Delta^{(i)}}, \quad (3.13)$$

where  $\phi^{(i)}$ ,  $i = 1, 2, 3$ , is one of the three fields in (B.26) with dimension  $\Delta^{(1)} = 0$ ,  $\Delta^{(2)} = 1 + \frac{2}{N+2}$  and  $\Delta^{(3)} = \frac{6}{N+2}$ . We can now use the same argument seen before, generalized to the non-Virasoro case [18]. In the limit  $x \rightarrow 0$ ,  $Z_{II}$  is described by a Bessel process of fractal dimension (3.5). Comparing (3.5) and (3.6) to (3.13), the  $G_N^{(i)}$  contributing to  $Z_{II}$  are the ones satisfying:

$$\Delta^{(i)} > 2\Delta_\varepsilon - \frac{2}{\kappa}. \quad (3.14)$$

For any  $N \geq 4$ , the above condition selects the fusion channels with  $\Delta^{(2)} = 1 - \frac{2}{N+2}$  and  $\Delta^{(3)} = \frac{2}{N+2}$ . We conclude that  $Z_{II}(x)$  is proportional to a linear combination of  $G_N^{(2)}(x)$ , and  $G_N^{(3)}$

$$Z_{II}(x) \propto G_N^{(2)}(x) + \alpha G_N^{(3)}(x). \quad (3.15)$$

In the case of symmetric boundary conditions, such as the ones (12|34|12|34) illustrated above, we can also set :

$$Z_I(x) = Z_{II}(1-x). \quad (3.16)$$

We obtain, for  $N \geq 4$ , the following expression:

$$\begin{aligned} \mathcal{P}_h(x) &= \frac{G_N^{(2)}(x) + \alpha G_N^{(3)}(x)}{G_N^{(2)}(x) + G_N^{(2)}(x) + \alpha \left( G_N^{(3)}(1-x) + G_N^{(3)}(1-x) \right)} \\ \mathcal{P}_v(x) &= \mathcal{P}_h(1-x) \end{aligned} \quad (3.17)$$

We could not determine the constant  $\alpha$ . Analogously to the determination of  $\beta$ , see (3.8), this requires to find the connection of a Fuchsian system. However, differently from the case  $N = 3$ , for  $N \geq 4$  this is a non-rigid rank 3 Fuchsian system and finding the connection of this system is a very hard problem, see the discussion in [29]. We let  $\alpha$  undetermined and we use it as a fit parameter in the comparison with Monte-Carlo results.

### 3.2 Measurements

We present the results for crossing probabilities taken for a rectangle of ratio  $r$  for the  $Z_3$  and  $Z_4$  spin models. By means of conformal map, see for instance [30], one finds the relation between  $r$  and  $x$  appearing in the previous formula:

$$r = \frac{K(x)}{K(1-x)}, \quad (3.18)$$

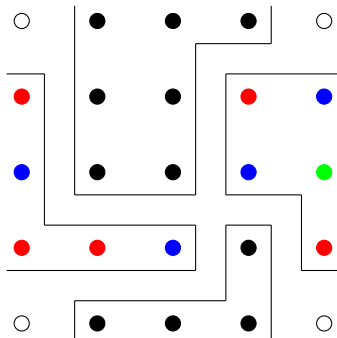
where  $K(x)$  is the complete elliptic integral of the first kind.

We give here some details on the measurements. For the  $Z_4$  models, very efficient cluster algorithms are available [31]. We have just to keep the cluster changes compatible

with the boundary conditions and this slows down the updates and limits the size we can simulate. For example, if during an update, a cluster is touching a boundary at the position  $i$  with the condition  $S_i = 1$  corresponding to  $\sigma_i = +$  and  $\tau_i = +$ , then this update can not be implemented. Indeed, any update<sup>1</sup> would change the sign of  $\sigma_i$  or  $\tau_i$  which would not preserve the boundary condition. We expect therefore non negligible finite size corrections to the measurements.

For each value of  $r$  and for each size  $L_h$ , we first made measurements of the autocorrelation time  $\tau(L_h, r)$ . Next we measure the probabilities  $P_h$  and  $P_v$  during a MC time  $10^6\tau(L_h, r)$  corresponding to  $10^6$  independent configurations. We performed measurements for  $r = 1, 1.2, 1.5, 2.0$ . For each value of  $r$ , we measure for  $L_h = 10, 20, 40, 80, 160, 320$  and  $640$ . For  $r = 1.5$  we also simulated  $L_h = 1280$ .

Note that on the square lattice, for a given configuration, we can have the condition  $P_h = P_v = 0$ . This corresponds to configuration with a corner. For example, the following configuration corresponding to  $L_h = L_v = 5$  with fixed boundary conditions,  $S_i = 1$  on top and bottom (showed as filled black circles) and  $S_i = 2, 3, 4$  on left and right (showed as filled red, blue or green circles) :



White circles on the upper/lower and left/right corners correspond to non connected spins. For this particular configuration, we see that each border is connected to a cluster but no cluster is crossing the lattice. In practice, we observe that there is a very small number of such configurations and this number (or the proportion of this number) decrease with the linear size. To take in account these few configurations, we define the number of crossings as in (3.1).

### 3.2.1 (1|23) Potts spin interface

We first present results for the crossing probabilities for the  $Q = 3$  Potts model with the conditions (1|23). In Tab. 1, we show the results for  $\mathcal{P}_h(r)/\mathcal{P}_v(r)$  as a function of  $r = L_h/L_v$ . In this table, the first result is the prediction from (3.9) and the second result is the estimate for our numerical data. We performed simulations for  $L_h \leq 640$  for  $r \geq 1$  and for  $L_v \leq 640$  for  $r \leq 1$ .

In practice, we observe that there are strong finite size corrections. We show an example for  $r = 1.5$  in Fig. 4 in which we plot  $\mathcal{P}_h(r)/\mathcal{P}_v(r)$  vs.  $1/L_h$ . The value is expected to converge in the zero limit to the value 0.0508417. Taking a fit of the form  $a+b/L_h^c$ , with data in the range  $[0 : 0.02]$ , we obtain  $a = 0.051(9)$  which is compatible with

<sup>1</sup>The update is done by considering separately an update of the  $\sigma$ 's or the  $\tau$ 's, see [31] for details.

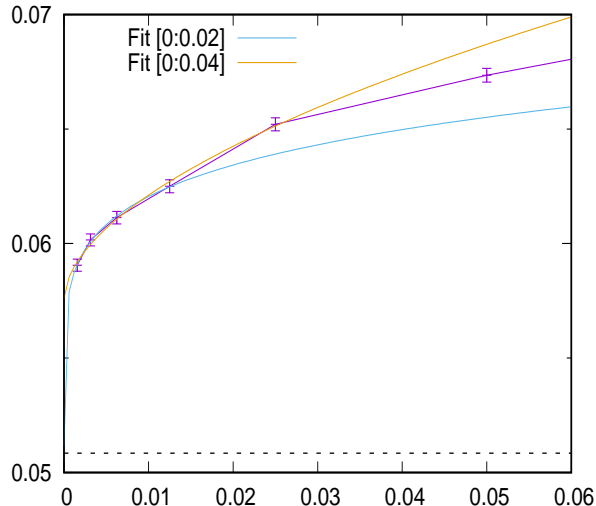


**Figure 4.**  $\mathcal{P}_h(r)/\mathcal{P}_v(r)$  as a function of  $1/L_h$  for the conditions (1|23) for the  $Q = 3$  Potts model and for  $r = 1.5$ .

the expected value. If we took a fit in the range  $[0 : 0.04]$ , then we obtain  $a = 0.058(1)$  which is close to the expected value but not any more compatible. We also found that for all the values of  $r$ , the exponent  $c$  is always very small, making a precise determination difficult.

$r$	From (3.9)	$\mathcal{P}_h(r)/\mathcal{P}_v(r)$
2.0	0.00542833	0.0059 (3)
1.5	0.0508417	0.051 (9)
1.1	0.354786	0.373 (6)
1.0	0.618034	0.655 (6)
$1/1.1=0.909091$	1.07661	1.19 (6)
$1/1.5 = 0.666667$	7.51285	8.2 (1)
$1/2 = 0.5$	70.3653	75 (6)

**Table 1.**  $\mathcal{P}_h(r)/\mathcal{P}_v(r)$  in function of  $r = L_v/L_h$ .

### 3.2.2 $Z_4$ spin model

In Fig. 5, we show our numerical results for  $\mathcal{P}_v(r)$ , the probability of having a cluster crossing from the top to the bottom, as a function of  $1/L_h$  for the condition (1|234) and (12|34). The figure contains data for  $r = 1, 2$  in the upper left panel, for  $r = 1.5$  in the upper right panel and for  $r = 2.0$  in the lower panel.

We first consider the data for the boundary condition (1|234). In that case, for both aspect ratios, we observe that  $\mathcal{P}_v(r)$  first increases as a function of  $L_h$  and then falls down. The fact that it does not converge is consistent with our previous observation that these boundary conditions are not the conformal boundary conditions, as discussed in Section (2.3), see Figure 2.

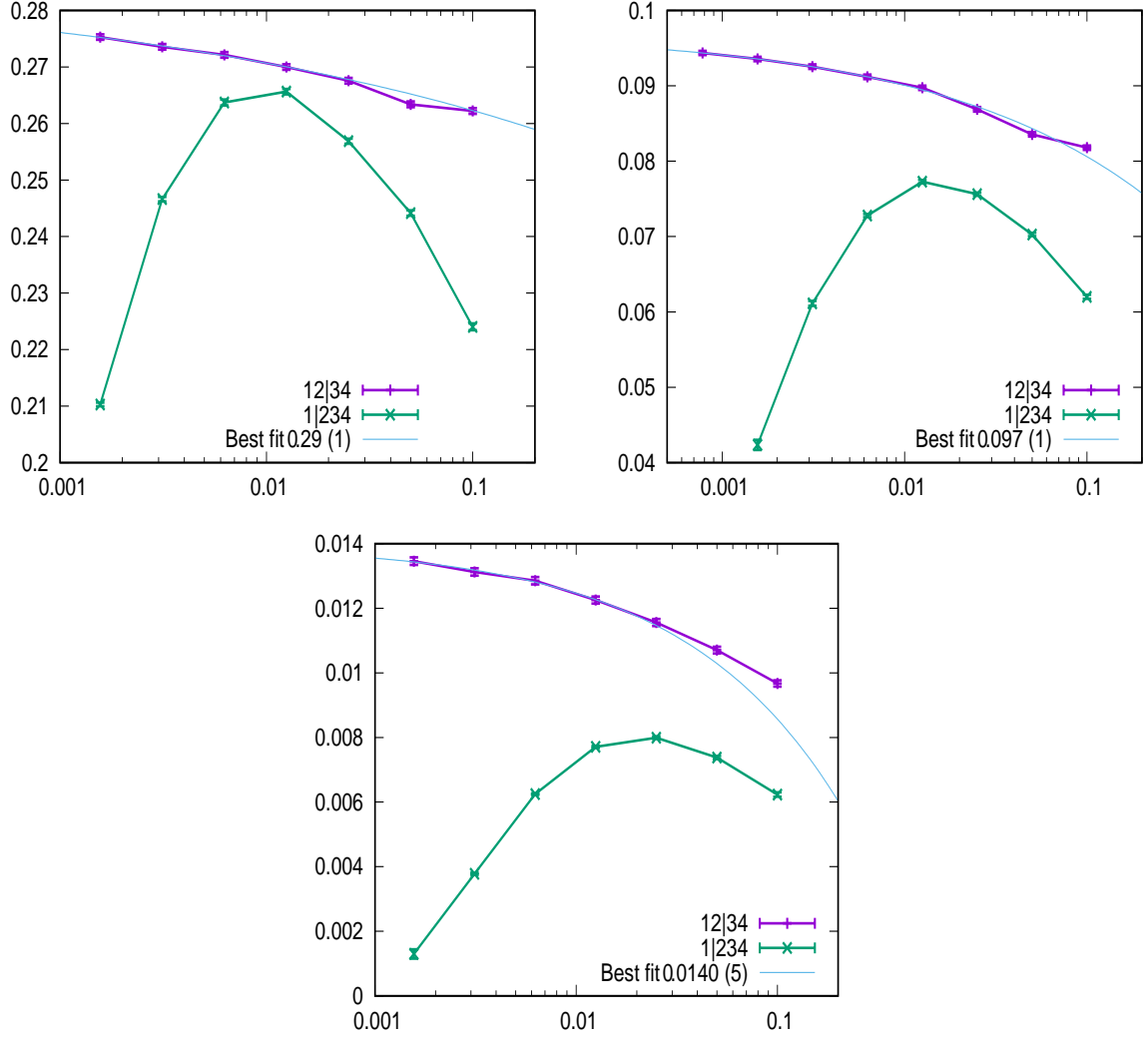


**Figure 5.**  $\mathcal{P}_v(r)$  as a function of  $1/L_h$  for the conditions (1|234) and (12|34).  $r = 1.2$  on the upper left,  $r = 1.5$  on the upper right and  $r = 2.0$  on the bottom.

Next, we consider the case with the boundary condition (12|34). In order to take in account finite size effects, we consider a fit to the form

$$\mathcal{P}_h(L_h, r) = \mathcal{P}_h(\infty, r) + \alpha(r)L_h^{-\beta(r)}. \quad (3.19)$$

In Fig. 5, we also show a fit of this for the boundary condition (12|34). It converges nicely but the asymptotic limit still depends on the smallest value we keep for  $L_h$ . For instance for  $r = 1.5$ , we obtained, for the following choices of smallest value  $L_h$  :

$$L_h \geq 20 \rightarrow \beta(1.5) \simeq 0.46(3) ; \mathcal{P}_h(\infty, 1.5) = 0.096(1) \quad (3.20)$$

$$L_h \geq 40 \rightarrow \beta(1.5) \simeq 0.46(7) ; \mathcal{P}_h(\infty, 1.5) = 0.096(1) \quad (3.21)$$

$$L_h \geq 80 \rightarrow \beta(1.5) \simeq 0.29(4) ; \mathcal{P}_h(\infty, 1.5) = 0.098(1) \quad (3.22)$$

$$L_h \geq 160 \rightarrow \beta(1.5) \simeq 0.37(1) ; \mathcal{P}_h(\infty, 1.5) = 0.097(1) \quad (3.23)$$

By extrapolation, we determine

$$\mathcal{P}_h(\infty, 1.2) = 0.29(1) ; \mathcal{P}_h(\infty, 1.5) = 0.097(2) ; \mathcal{P}_h(\infty, 2.0) = 0.0135(10). \quad (3.24)$$

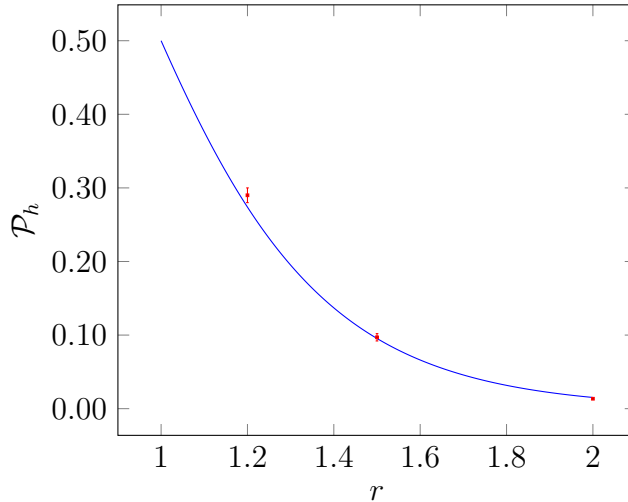


**Figure 6.** The (blue) line is the crossing probability (3.17) as a function of the rectangle ratio  $r$ , see (3.18). The value of the parameter  $\alpha$  has been set by minimising the deviation from the numerical data from the prediction with  $\alpha = 0.325$ . The (red) squares are the results for the asymptotic limit  $\mathcal{P}_h(\infty, r)$  obtained from (3.19).

We have also run measurements for  $r = 1$ . For the condition (12|34), we have a symmetry which ensure that  $\mathcal{P}_h(\infty, 1) = \mathcal{P}_v(\infty, 1)$ .

We can now compare the above results with the theoretical prediction (3.17) for  $N = 4$ . This prediction is a function of a unknown constant  $\alpha$ . We thus perform a fit minimising, in function of  $\alpha$ , the relative difference between the measured data for  $r = 1.2, 1.5$  and  $2.0$  and the prediction. The minimal deviation is obtained for  $\alpha = 0.325$  at which the (3.17) gives :

$$\mathcal{P}_h(1.2) = 0.273889 \ ; \ \mathcal{P}_h(1.5) = 0.0954003 \ \mathcal{P}_h(2) = 0.0152398 . \quad (3.25)$$

These values are in fact rather close to the measured values, see Fig. 6.

## 4 Conclusion

In this paper we have considered spin interfaces in the  $Z_3$  ( $Q = 3$  state Potts) and in the  $Z_4$  parafermionic spin models. As shown in Figure 1 and in Figure 2, the scaling behavior of different spin interfaces is determined by two fractal dimensions, respectively  $d_f = 17/12$  and  $d_f \sim 0.98$ , and  $d_f = 3/2$ ,  $d_f = 17/12$ . In particular the dimension  $d_f = 17/12$  was obtained for  $Z_4$  spin models in previous works by using the SLE/ECFT correspondence, whose validity is thus supported by the numerical results presented here. We further investigated this correspondence by studying the crossing probabilities of spin interfaces. We compute the  $Z_N$  crossing probability, given in (3.9) for  $N = 3$  and in (3.17) for  $N \geq 4$ , where the extended symmetry starts to play an important role. Note that the formula (3.17) is given in terms of a parameter  $\alpha$  that we could not fix. The parafermionic conformal blocks entering the (3.17) have been computed by using the  $SU(2)_N$  coset description of the parafermionic CFT, and in particular by solving the Knizhnik-Zamolodchikov system of rank 3. Full details are provided in the Appendices.

For the  $Q = 3$  spin Potts model, we have verified that the parafermionic conformal blocks coincides with the one of the Virasoro algebra and that the formula (3.9) is a special case of the crossing formulas given in [3]. Our numerical data, shown in Table 1 are in good agreement with the prediction (3.9). The comparison between the numerical results for  $N = 4$ , and the prediction (3.17) is shown in (3.24)-(3.25) and in Figure 6. Taking into account the presence of finite size effects, the agreement between the numerical and theoretical prediction is good.

## A $Z_N$ parafermionic theory

The  $Z_N$  theories have central charge:

$$c_N = \frac{2(N-1)}{N+2} \quad (\text{A.1})$$

and describe critical theories with dihedral group symmetry  $D_N = Z_N \otimes (Z_2)^N$  [32]. The Hilbert space of the  $Z_N$  theories is constructed from the representations of the parafermionic algebra. The representation modules can be split into two sectors [33], the disorder and the charge sector, associated respectively to the  $(Z_2)^N$  and to the  $Z_N$  element of the group  $D_N$ . Here we are interested in the charge sector, that contains  $\lfloor \frac{N}{2} \rfloor + 1$  representation modules  $\mathcal{V}_j$ , where  $\lfloor x \rfloor$  is the integer part of  $x$ :

$$\text{Parafermionic primaries: } \Phi^{\pm j} \begin{cases} j = 0, 1, \dots, \frac{N-1}{2} & (N \text{ odd}) \\ j = 0, \frac{1}{2}, \dots, \frac{N}{4} & (N \text{ even}) \end{cases} \quad (\text{A.2})$$

Each module  $\mathcal{V}_j$  is formed by the descendants of:

$$\Phi^{\pm j}, \quad j = 0, 1, \dots, \frac{N-1}{2} \quad N \text{ odd}, \quad j = 0, \frac{1}{2}, \dots, \frac{N}{4} \quad N \text{ even} \quad (\text{A.3})$$

that have  $Z_N$  charge  $j$  (defined mod  $N$ ) and conformal dimension:

$$\Delta_j = \frac{j(N-2j)}{N(N+2)}. \quad (\text{A.4})$$

When  $j = -j \pmod{N}$ , the two fields  $\Phi^{\pm j}$  coincide.

Besides the Identity,  $\text{Id} = \Phi^0$ , there are  $\lfloor \frac{N}{2} \rfloor$  Virasoro primaries  $\varepsilon^{(j)}$  with zero  $Z_N$  charge. They appear in  $\mathcal{V}_j$  as the lowest dimension descendant. Among these neutral fields, the field  $\varepsilon = \varepsilon^{(1)}$  has the lowest dimension given in (3.10).

The above field is the one that was considered in [14, 15] as the boundary changing condition field generating the SLE interface. Accordingly we expect the crossing probability associated to these SLE interfaces to be given by the conformal block (3.12).

For  $N = 2$  (Ising) and  $N = 3$  (3-state Potts), one can show that  $G_{N(=2,3)}(x)$  satisfies the same correlations functions as the one of the corresponding Virasoro minimal model. In [14] this was explicitly shown for  $N = 3$  and we provide below also the demonstration for  $N = 2$ , missing in [14].

### A.1 Ising case, $N = 2$

In this case one has the  $\mathcal{V}_0$  (Neveu-Schwartz sector) and  $\mathcal{V}_{\frac{1}{2}}$  (Ramond sector) representation module. We denote as  $[\Phi^0]$  a general (parafermionic) descendants field in identity field module  $\mathcal{V}_0$ . The (para)fermionic current  $\psi(z)$  satisfies the OPE

$$\psi(z)\psi(0) = \frac{1}{z} + 2 z^2 T^{Z_2}(0), \quad (\text{A.5})$$

where  $T^{Z_2}$  is the stress-energy tensor

$$T^{Z_2}(z) [\Phi^0] (0) = \sum_{n=-\infty}^{\infty} \frac{1}{z^{n+2}} L_n^{Z_2} [\Phi^0] (0) \quad (\text{A.6})$$

whose modes  $L_n^{Z_2}$  generate a  $c = \frac{1}{2}$  Virasoro algebra. The  $\psi$  modes acting in  $\mathcal{V}_0$  can be expressed as:

$$A_{-\frac{1}{2}+n} [\Phi^0] (0) = \frac{1}{2\pi i} \oint_{\mathcal{C}_0} dz z^{n-1} \psi(z) [\Phi^0] (0), \quad (\text{A.7})$$

where  $\mathcal{C}_z$  is a contour encircling  $z$ . The current modes satisfy the (anti-)commutation relation:

$$\{A_{-\frac{1}{2}+n}, A_{-\frac{1}{2}+m}\} = \delta_{n+m,1}, \quad (\text{A.8})$$

that is a direct consequence of the fact that  $\psi(z)$  is a free fermion. As previously said,  $\varepsilon$  appears as a parafermionic descendant. In the case  $N = 2$  it appears in the identity module:

$$\varepsilon = A_{-\frac{1}{2}} \Phi^0. \quad (\text{A.9})$$

Note that, setting  $n = 0, m = 0$  in (A.8), one gets:

$$A_{-\frac{1}{2}} A_{-\frac{1}{2}} \Phi^0 = A_{-\frac{1}{2}} \varepsilon = 0. \quad (\text{A.10})$$

From (A.7) and using standard contour integral manipulations, one finds that:

$$\begin{aligned} & \frac{1}{(2\pi i)^2} \oint_{\mathcal{C}_0} dz \oint_{\mathcal{C}_z} (z)^{n-1} (z')^{m-1} (z-z')^{-2} \psi(z) \psi(z') [\Phi^0] (0) = \\ & = \sum_{k=0}^{\infty} (-1)^k \binom{-2}{k} \left( A_{-\frac{1}{2}+n-2-k} A_{-\frac{1}{2}+m+k} + A_{-\frac{1}{2}+m-2-k} A_{-\frac{1}{2}+n+k} \right) \end{aligned} \quad (\text{A.11})$$

Using (A.5) and the Cauchy theorem, one obtains the following relations between the  $\psi$  and  $T^{Z_2}$  modes:

$$\begin{aligned} & \sum_{k=0}^{\infty} (-1)^k \binom{-2}{k} \left( A_{-\frac{1}{2}+n-2-k} A_{-\frac{1}{2}+m+k} + A_{-\frac{1}{2}+m-2-k} A_{-\frac{1}{2}+n+k} \right) = \\ & \frac{(m-1)(m-2)}{2} \delta_{n+m,3} + 2 L_{n+m-3}^{Z_2}. \end{aligned} \quad (\text{A.12})$$

By setting  $n = 1, m = 1$  and  $n = 1, m = 0$  in the above formula and using the commutations (A.8), one obtains:

$$\begin{aligned} (L_{-1}^{Z_2})^2 \varepsilon &= \left( A_{-\frac{3}{2}} A_{\frac{1}{2}} + 2 A_{-\frac{5}{2}} A_{+\frac{3}{2}} \right) A_{-\frac{3}{2}} A_{\frac{1}{2}} \varepsilon = 2 A_{-\frac{5}{2}} A_{\frac{1}{2}} \varepsilon \\ L_{-2}^{Z_2} \varepsilon &= \left( \frac{1}{2} A_{-\frac{3}{2}} A_{-\frac{1}{2}} + \frac{3}{2} A_{-\frac{5}{2}} A_{\frac{1}{2}} \right) \varepsilon = \frac{3}{2} A_{-\frac{5}{2}} A_{\frac{1}{2}} \varepsilon. \end{aligned} \quad (\text{A.13})$$

This implies:

$$\left( (L_{-1}^{Z_2})^2 - \frac{4}{3} L_{-2}^{Z_2} \right) \varepsilon = 0, \quad (\text{A.14})$$

that coincides with the second-order null vector condition of the minimal model at  $c = \frac{1}{2}$ .

## B Computation of $G_N(x)$ for $N \geq 4$

We show now how to compute  $G_N(z)$  for any  $N$  by using the coset  $\frac{SU(2)_N}{U(1)_N}$  description of the charge sector. In order to fix conventions and notations, let us first briefly review the  $U(1)_N$  and  $SU(2)_N$  CFTs.

The  $U(1)_N$  theory is a CFT with a current  $J = i\partial\phi$  of conformal dimension one, where  $\phi$  is a free Gaussian field. The current modes  $J_n$  form the Heisenberg algebra:

$$[J_n, J_m] = n\delta_{n+m,0}. \quad (\text{B.1})$$

The stress energy-tensor:

$$T^{U(1)} = \frac{1}{2} : J J :, \quad (\text{B.2})$$

forms a Virasoro algebra with central charge:

$$c^{U(1)} = 1. \quad (\text{B.3})$$

The  $U(1)_N$  primary fields are the vertex fields  $e^{i\frac{m}{\sqrt{N}}\phi}$  labeled by  $m \in \mathbb{Z}/2$ , defined modulo  $N$ , that have conformal dimension  $\Delta_m^{U(1)}$ :

$$\Delta_m^{U(1)} = \frac{m^2}{N}. \quad (\text{B.4})$$

The  $SU(2)_N$  theory is based on the algebra formed by three conserved current  $J^a$ ,  $a = 0, +, -$  of conformal dimension one:

$$[J_n^a, J_m^b] = f_c^{ab} J_{n+m}^c + \frac{Nn}{2} q^{ab} \delta_{n+m} \quad (\text{B.5})$$

with the structure constants  $f_0^{\pm,\mp} = \pm 2$ ,  $f_0^{0,\pm} = \pm 2$  and the Killing form  $q^{a,b}$  is  $q^{0,0} = 1$ ,  $q^{+,-} = q^{-,+} = 2$ . The stress-energy tensor is given by:

$$T^{SU(2)} = \frac{1}{N+2} q_{a,b} : J^a J^b :, \quad (\text{B.6})$$

where  $::$  denotes the regular part and it generates a Virasoro algebra with central charge:

$$c^{SU(2)_N} = \frac{3N}{N+2}. \quad (\text{B.7})$$

The representation module  $\mathcal{V}_l^{SU(2)}$ ,  $l \in \frac{\mathbb{N}}{2}$ , contains the Virasoro primary fields  $\phi_m^j$  that have conformal dimension:

$$\Delta_j^{SU(2)} = \frac{j(j+1)}{N+2} \quad (\text{B.8})$$

and transform under the action of  $J_0^a$  as the  $su(2)$  Lie algebra weights  $|l, m\rangle$ ,  $m = -l, -l+1, \dots, l$ . In particular, the  $SU(2)$  Ward identities are encoded in the following OPE:

$$J^a(x)\phi_m^j(0) = \frac{1}{x} \sum_{m'=-j}^j (t^a)^{(j)}_{m,m'} \phi_{m'}^j(0) + \text{Regular terms}, \quad (\text{B.9})$$

where  $(t^a)^{(j)}_{m,m'}$  is the  $(2j+1) \times (2j+1)$  matrix in the representation  $j$ . As  $\langle J(x) \prod_i \phi_{m_i}^{j_i} \rangle \sim x^{-2}$  for  $x \rightarrow \infty$ , the above OPE implies:

$$\sum_i (t^a)^{(j_i)}_{m_i, m'_i} \left\langle \prod_i \phi_{m'_i}^{j_i}(x_i) \right\rangle = 0 \quad (\text{B.10})$$

From (B.6) one can show also that the  $SU(2)$  conformal blocks satisfy the Knizhnik-Zamolodchikov equations [34]:

$$\left[ \partial_{x_i} + \sum_{j \neq i} \frac{q_{a,b}}{z - z_i} (t^a)^{(j)} (t^b)^{(i)} \right] \left\langle \prod_l \phi_{m_l}^{l_i} \right\rangle = 0 \quad (\text{B.11})$$

In the coset construction  $\frac{SU(2)_N}{U(1)_N}$ , the stress-energy tensor  $T^{Z_N}$  of  $Z_N$  satisfies the relation

$$T^{SU(2)} = T^{U(1)} + T^{Z_N}, \quad (\text{B.12})$$

and the primaries fields of the three CFTs are related by:

$$\phi_{\pm j}^j = \Phi^j e^{i \frac{\pm j}{\sqrt{N}} \phi}, \quad \phi_0^j = \varepsilon^{(j)} \quad (\text{B.13})$$

In particular we have for the  $\varepsilon = \varepsilon^{(1)}$  fields in (3.12):

$$\varepsilon = \phi_0^1 \quad (\text{B.14})$$

## B.1 $SU(2)_N$ conformal blocks and Knizhnik-Zamolodchikov equation

By using (B.14), we will write the function  $G_N(z)$  in (3.12) as:

$$G_N(x) = \langle \phi_0^1(0) \phi_0^1(x) \phi_0^1(1) \phi_0^1(\infty) \rangle, \quad (\text{B.15})$$

and we will solve the corresponding equation (B.11).

### B.1.1 Coulomb gas representation of the rank 3 KZ system

The solution of the KZ system can be given in terms of Coulomb gas integrals [35, 36]. Take the more general function

$$G^{\{m_i\}}(x) = \langle \phi_{m_1}^1(0) \phi_{m_2}^1(x) \phi_{m_3}^1(1) \phi_{m_4}^1(\infty) \rangle, \quad \sum_i m_i = 0. \quad (\text{B.16})$$

This function lives in the  $SU(2)$  singlet of the fusion  $1 \otimes 1 \otimes 1 \otimes 1$  of four spin-1 representations. In this case the invariant space has dimension 3, i.e. it is spanned by three independent tensors  $T_{\{m_i\}}^{(l)}$  with  $l = 0, 1, 2$ :

$$T_{\{m_i\}}^{(l)} = \frac{1}{2l+1} \sum_{m=-l}^l \langle l, m | 1, m_1; 1, m_2 \rangle \langle l, -m | 1, m_3; 1, m_4 \rangle. \quad (\text{B.17})$$

where  $\langle j_3, m_3 | j_1, m_1; j_2, m_2 \rangle$  are the  $SU(2)$  Clebsh-Gordan coefficients. As usual for conformal blocks, specifying the primaries  $\{m_i\}$  does not completely determine the function: we need to specify the quantum numbers  $j$  and  $m$  of the  $\Phi_m^j$  in the internal channel. In the following we will use the basis of [36]. Note that we could equivalently choose the one in [35]. In the tensor basis  $T_{\{m_i\}}^{(l)}$ , we have:

$$G^{\{m_i\}}(z) = \left[ \sum_{l=0}^2 T_{\{m_i\}}^{(l)} g^{(l)}(z) \right], \quad (\text{B.18})$$

where the functions  $f^{(l)}(z)$  are expressed via Coulomb gas integrals, see below. Using in (B.18) the Clebsh-Gordan coefficients

$$\begin{aligned} \langle l=0, m=0 | 1, m_1=0; 1, m_2=0 \rangle &= -\sqrt{\frac{1}{3}}, \\ \langle l=2, m=0 | 1, m_1=0; 1, m_2=0 \rangle &= \sqrt{\frac{2}{3}}, \\ \langle l=1, m=0 | 1, m_1=0; 1, m_2=0 \rangle &= 0, \end{aligned} \quad (\text{B.19})$$

one can see that  $G_N(x)$  gets contribution from  $g^{(0)}(x)$  and  $g^{(2)}(x)$ , that are given in [36]<sup>2</sup>:

$$g^{(i)}(x) = z^{\frac{2}{N+2}} (1-x)^{\frac{2}{N+2}} \int_{\mathcal{C}} du_1 du_2 f^{(i)}(u_1, u_2, x), \quad i=0, 2, \quad (\text{B.20})$$

where

$$\begin{aligned} f^{(0)}(u_1, u_2, x) &= u_1^{-\frac{2}{N+2}-1} u_2^{-\frac{2}{N+2}-1} (u_1-1)^{-\frac{2}{N+2}} (u_2-1)^{-\frac{2}{N+2}} \\ &\quad (u_1-x)^{-\frac{2}{N+2}-1} (u_2-x)^{-\frac{2}{N+2}-1} (u_1-u_2)^{\frac{2}{N+2}}, \\ f^{(2)}(u_1, u_2, z) &= u_1^{-\frac{2}{N+2}} u_2^{-\frac{2}{N+2}} (u_1-1)^{-\frac{2}{N+2}-1} (u_2-1)^{-\frac{2}{N+2}-1} \\ &\quad (u_1-x)^{-\frac{2}{N+2}} (u_2-x)^{-\frac{2}{N+2}} (u_1-u_2)^{\frac{2}{N+2}}. \end{aligned} \quad (\text{B.21})$$

In (B.20),  $\mathcal{C}$  is a closed contour in the Riemann surface associated to the multi-valued functions  $f^{(i)}(u_1, u_2, x)$ . The integrals:

$$\begin{aligned} I_{\mathcal{C}_1}^{(i)}(x) &= x^{\frac{2}{N+2}+i} (1-z)^{\frac{2}{N+2}} \int_0^x du_1 \int_0^{u_1} du_2 f^{(i)}(u_1, u_2, x) \\ I_{\mathcal{C}_2}^{(i)}(x) &= x^{\frac{2}{N+2}+i} (1-z)^{\frac{2}{N+2}} \int_0^x du_1 \int_1^\infty du_2 f^{(i)}(u_1, u_2, x) \\ I_{\mathcal{C}_3}^{(i)}(x) &= x^{\frac{2}{N+2}+i} (1-z)^{\frac{2}{N+2}} \int_1^\infty du_1 \int_1^{u_1} du_2 f^{(i)}(u_1, u_2, x), \end{aligned} \quad (\text{B.22})$$

correspond to the conformal blocks that transform diagonally under the monodromy around the  $x=0$  singularity and form a basis, the  $s$ -channel basis, on which the functions  $g^{(i)}(x)$  can be expanded:

$$g^{(i)}(x) \rightarrow \{I_{\mathcal{C}_1}^{(i)}(x), I_{\mathcal{C}_2}^{(i)}(x), I_{\mathcal{C}_3}^{(i)}(x)\}, \quad (\text{B.23})$$

---

<sup>2</sup>We use different notation from [36]. For instance, the functions  $g^{(k)}(x)$  here corresponds to the  $f^{(k+1)}(\eta)$  given in Eq. (3.6) of [36]

One can read the small  $x$  asymptotic behavior of  $I_{\mathcal{C}_j}^{(i)}(x)$ :

$$\begin{aligned} I_{\mathcal{C}_3}^{(0)}(x) &\sim x^{\frac{2}{N+2}+2} (1 + \dots), & I_{\mathcal{C}_3}^{(2)}(x) &\sim x^{\frac{2}{N+2}} (1 + \dots) \\ I_{\mathcal{C}_2}^{(0)}(x) &\sim x^{1-\frac{2}{N+2}} (1 + \dots), & I_{\mathcal{C}_2}^{(2)}(x) &\sim x^{1-\frac{2}{N+2}} (1 + \dots) \\ I_{\mathcal{C}_1}^{(0)}(x) &\sim x^{-\frac{4}{N+2}} (1 + \dots), & I_{\mathcal{C}_1}^{(2)}(x) &\sim x^{-\frac{4}{N+2}+2} (1 + \dots) \end{aligned} \quad (\text{B.24})$$

The exponents

$$\alpha_1 = -\frac{4}{N+2}, \quad \alpha_2 = 1 - \frac{2}{N+2}, \quad \alpha_3 = \frac{N}{N+2} \quad (\text{B.25})$$

correspond respectively to the fusion channels:

$$\phi_0^1 \times \phi_0^1 = \phi_0^0 + J_{-1}^\pm \phi_{\mp 1}^1 + \phi_0^2, \quad (\text{B.26})$$

Notice that the fusion coefficient  $\phi_0^1 \times \phi_0^1 \rightarrow \phi_0^1$  vanishes with the corresponding Clebsch-Gordon coefficient, see (B.19).

### B.1.2 Solution of the rank 3 KZ by the Frobenius method

We have seen that the solutions of the rank 3 system are expressed in terms of bidimensional integrals whose evaluation requires to compute double infinite sums of  ${}_3F_2$  hypergeometric functions. We verified that the convergence of these sums is quite slow. A more efficient method is to use the Frobenius method to find a series expansion of the solution. We notice that this method for a Fuchsian system of rank 3 has been also applied in [37].

In our conventions the matrix appearing in (B.11) have the form:

$$(t^+)^{(1)} = \begin{bmatrix} 0 & -i & 0 \\ 0 & 0 & -2i \\ 0 & 0 & 0 \end{bmatrix}, \quad (t^-)^{(1)} = \begin{bmatrix} 0 & 0 & 0 \\ 2i & 0 & 0 \\ 0 & i & 0 \end{bmatrix}, \quad (t^0)^{(1)} = \begin{bmatrix} 1 & 0 & 0 \\ 0 & 0 & 0 \\ 0 & 0 & -1 \end{bmatrix}. \quad (\text{B.27})$$

Using the above matrices, one can verify that the (B.11) is a system of first-order differential equation that couples the conformal block (B.15) with other conformal blocks containing four spin-1 representation. Using the Ward identities (B.10), one can show that the space of functions appearing in the KZ system is spanned by three independent functions. We take as a basis the following ones:

$$a(x) = \langle \phi_{-1}^1(0) \phi_1^1(x) \phi_{-1}^1(1) \phi_1^1(\infty) \rangle \quad (\text{B.28})$$

$$b(x) = \langle \phi_0^1(0) \phi_0^1(x) \phi_{-1}^1(1) \phi_1^1(\infty) \rangle \quad (\text{B.29})$$

$$G_N(x) = \langle \phi_0^1(0) \phi_0^1(x) \phi_0^1(1) \phi_0^1(\infty) \rangle \quad (\text{B.30})$$

In the basis of functions  $(a(x), b(x), G_N(x))$ , the KZ equation (B.11) takes the form:

$$\frac{N+2}{2} \partial_x F = \frac{1}{x} A_0 F + \frac{1}{x-1} A_1 F, \quad (\text{B.31})$$

where  $F$  is defined by  $(a(x), b(x), G_N(x))^t$  and

$$A_0 = \frac{2}{N+2} \begin{bmatrix} -1 & 2 & 0 \\ 0 & -1 & 2 \\ 0 & 1 & 0 \end{bmatrix}, \quad A_1 = \frac{2}{N+2} \begin{bmatrix} 1 & 0 & 0 \\ -\frac{1}{2} & -1 & 0 \\ \frac{1}{2} & 0 & -2 \end{bmatrix}. \quad (\text{B.32})$$

The Fuchsian system (B.31) implies that the  $G_N(x)$  satisfies a 3rd order differential equation of Fuchsian type:

$$\left( \partial_x^3 + \frac{h_2(N, x)}{x(x-1)} \partial_x^2 + \frac{h_1(N, x)}{x^2(x-1)^2} \partial_x + \frac{h_0(N, x)}{x^2(x-1)^3} \right) G_N(x) = 0, \quad (\text{B.33})$$

with:

$$\begin{aligned} h_2(N, x) &= \frac{2(-7 - N + (11 + 2N)x)}{(N+2)}, \\ h_1(N, x) &= \frac{2(16 + 2N - (72 + 17N + N^2)x + (56 + 16N + N^2)x^2)}{(N+2)^2}, \\ h_0(N, x) &= \frac{4(24 + 3N - (48 + 5N)x + (24 + 4N)x^2)}{(N+2)^3}. \end{aligned} \quad (\text{B.34})$$

The corresponding vector of solutions  $G_N^{(i)}(z)$ ,  $i = 1, 2, 3$  can be given as an expansion around one of the branch singularities at  $x = 0, 1$  and  $x = \infty$ . Expanding around the  $x = 0$  singularities, the solutions take the form

$$G_N^{(i)}(x) = x^{\alpha_i} \sum_{n=0}^{\infty} p_n^{(i)}(N) x^n. \quad (\text{B.35})$$

In the above equation  $\alpha_i$  takes one of the values of the  $A_0$  eigenvalues

$$A_0 \sim \text{diag}[\alpha_1, \alpha_2, \alpha_3], \quad (\text{B.36})$$

that are given in (B.25). For each  $\alpha_i$ , the coefficients  $p_n^{(i)}(N)$  in (B.35) can be obtained very efficiently by using the Frobenius method for Fuchsian equations. For  $N = 4$ , that is the value at which we compare the analytical formula (3.17) to numerical simulations, we find:

$$\begin{aligned} G_4^{(1)}(x) &= x^{-\frac{2}{3}} \left( 1 + \frac{2}{9}x^2 + \frac{2}{9}x^3 + \frac{103}{486}x^4 + \frac{49}{253}x^5 + \dots \right) \\ G_4^{(2)}(x) &= x^{\frac{2}{3}} \left( 1 + \frac{2}{3}x + \frac{5}{9}x^2 + \frac{40}{81}x^3 + \frac{110}{243}x^4 + \frac{308}{729}x^5 + \dots \right), \\ G_4^{(3)}(x) &= x^{\frac{1}{3}} \left( 1 + \frac{1}{2}x + \frac{11}{27}x^2 + \frac{13}{36}x^3 + \frac{161}{486}x^4 + \frac{301}{971}x^5 + \dots \right). \end{aligned} \quad (\text{B.37})$$

## Acknowledgments

We thank Flavia Albarracin for contributing at an early stage of this project and Nina Javerzat and Jacopo Viti for useful discussions. YF acknowledges the support by the QuantiXLie Center of Excellence, a project co-financed by the Croatian Government and European Union through the European Regional Development Fund - the Competitiveness and Cohesion Operational Programme (Grant KK.01.1.1.01.0004). R.S. acknowledges the hospitality of the International Institute of Physics (Natal) where part of this work has been done.

## References

- [1] M. Picco, R. Santachiara and A. Sicilia, *Geometrical properties of parafermionic spin models*, *Journal of Statistical Mechanics: Theory and Experiment* (2009) P04013, [[0812.3526](#)].
- [2] M. Picco and R. Santachiara, *Critical interfaces of the Ashkin-Teller model at the parafermionic point*, *Journal of Statistical Mechanics: Theory and Experiment* (2010) P07027, [[1005.0493](#)].
- [3] S. M. Flores, J. J. H. Simmons, P. Kleban and R. M. Ziff, *A formula for crossing probabilities of critical systems inside polygons*, *Journal of Physics A: Mathematical and Theoretical* **50** (Jan, 2017) 064005.
- [4] M. Picco, S. Ribault and R. Santachiara, *On four-point connectivities in the critical 2d Potts model*, *SciPost Phys.* **7** (2019) 44.
- [5] Y. He, J. L. Jacobsen and H. Saleur, *Geometrical four-point functions in the two-dimensional critical  $Q$ -state Potts model: The interchiral conformal bootstrap*, [2005.07258](#).
- [6] N. Javerzat, M. Picco and R. Santachiara, *Two-point connectivity of two-dimensional critical  $Q$ -Potts random clusters on the torus*, *Journal of Statistical Mechanics: Theory and Experiment* **2020** (Feb, 2020) 023101.
- [7] N. Javerzat, M. Picco and R. Santachiara, *Three- and four-point connectivities of two-dimensional critical  $Q$ -Potts random clusters on the torus*, *Journal of Statistical Mechanics: Theory and Experiment* **2020** (may, 2020) 053106.
- [8] N. Javerzat, S. Grijalva, A. Rosso and R. Santachiara, *Topological effects and conformal invariance in long-range correlated random surfaces*, [2005.11830](#).
- [9] O. Schramm, *Scaling limits of loop-erased random walks and uniform spanning trees*, *Israel Journal of Mathematics* **118** (Dec, 2000) 221–288.
- [10] M. Bauer and D. Bernard,  *$SLE_\kappa$  growth processes and conformal field theories*, *Physics Letters B* **543** (2002) 135 – 138.
- [11] E. Bettelheim, I. A. Gruzberg, A. W. W. Ludwig and P. Wiegmann, *Stochastic Loewner Evolution for Conformal Field Theories with Lie Group Symmetries*, *Phys. Rev. Lett.* **95** (Dec, 2005) 251601.
- [12] K. Sakai, *Multiple Schramm–Loewner evolutions for conformal field theories with Lie algebra symmetries*, *Nuclear Physics B* **867** (2013) 429 – 447.
- [13] A. Zamolodchikov and V. Fateev, *Nonlocal (parafermion) currents in two-dimensional conformal quantum field theory and self-dual critical points in  $Z_N$ -symmetric statistical systems*, *JETP* **62** (August, 1985) 215.
- [14] R. Santachiara,  *$SLE$  in self-dual critical spin systems: CFT predictions*, *Nuclear Physics B* **793** (Apr, 2008) 396–424.
- [15] M. Picco and R. Santachiara, *Numerical Study on Schramm-Loewner Evolution in Nonminimal Conformal Field Theories*, *Physical Review Letters* **100** (Jan., 2008) 015704, [[0708.4295](#)].

- [16] M. Caselle, S. Lottini and M. A. Rajabpour, *Critical domain walls in the Ashkin–Teller model*, *Journal of Statistical Mechanics: Theory and Experiment* **2011** (Feb, 2011) P02039.
- [17] Y. Ikhlef and M. A. Rajabpour, *Discrete holomorphic parafermions in the Ashkin–Teller model and SLE*, *Journal of Physics A: Mathematical and Theoretical* **44** (Dec, 2010) 042001.
- [18] Y. Fukusumi, *Multiple Schramm-Loewner evolutions for coset Wess-Zumino-Witten models*, [1704.06006](#).
- [19] J. Ashkin and E. Teller, *Statistics of two-dimensional lattices with four components*, *Phys. Rev.* **64** (Sep, 1943) 178–184.
- [20] B. Nienhuis, *Critical behavior of two-dimensional spin models and charge asymmetry in the coulomb gas*, *Journal of Statistical Physics* **34** (Mar, 1984) 731–761.
- [21] H. Saleur, *Partition functions of the two-dimensional Ashkin-Teller model on the critical line*, *Journal of Physics A: Mathematical and General* **20** (1987) L1127.
- [22] R. J. Baxter, *Exactly solved models in statistical mechanics*. Academic Press, London, 1982.
- [23] V. A. Fateev and A. B. Zamolodchikov, *Conformal quantum field theory models in two dimensions having  $Z_3$  symmetry*, *Phys. Lett.* **92A** (1982) 37.
- [24] H. Au-Yang and J. H. H. Perk, *The chiral Potts models revisited*, *J. Stat. Phys.* **78** (1995) 17.
- [25] A. Gamsa and J. L. Cardy, *Schramm–Loewner evolution in the three-state Potts model—a numerical study*, *Journal of Statistical Mechanics: Theory and Experiment* (2007) P08020.
- [26] M. Picco and R. Santachiara, *unpublished, 2007*, .
- [27] M. Picco and R. Santachiara, *Critical interfaces and duality in the Ashkin Teller model*, *Phys. Rev.* **E83** (2011) 061124, [[1011.1159](#)].
- [28] M. Bauer, D. Bernard and K. Kytölä, *Multiple Schramm–Loewner Evolutions and Statistical Mechanics Martingales*, *Journal of Statistical Physics* **120** (Sep, 2005) 1125–1163.
- [29] V. Belavin, Y. Haraoka and R. Santachiara, *Rigid Fuchsian systems in 2-dimensional conformal field theories*, *Communications in Mathematical Physics* **365** (2019) 17–60, [[1711.04361](#)].
- [30] T. Blanchard and M. Picco, *Frozen into stripes: Fate of the critical ising model after a quench*, *Physical Review E* **88** (Sep, 2013) 032131.
- [31] S. Wiseman and E. Domany, *Cluster method for the Ashkin-Teller model*, *Physical Review E* **48** (1993) 4080.
- [32] A. B. Zamolodchikov and V. A. Fateev, *Nonlocal (parafermion) currents in two-dimensional conformal quantum field theory and self-dual critical points in zn symmetrical statistical models*, *Zh. Eksp. Teor. Fiz.; (USSR)* **89:2** (Aug, 1985) .
- [33] V. S. Dotsenko, J. L. Jacobsen and R. Santachiara, *Parafermionic theory with the symmetry  $Z_5$* , *Nuclear Physics B* **656** (Apr, 2003) 259–324.

- [34] V. Knizhnik and A. Zamolodchikov, *Current algebra and Wess-Zumino model in two dimensions*, *Nuclear Physics B* **247** (1984) 83 – 103.
- [35] V. Dotsenko, *Solving the  $SU(2)$  conformal field theory using the Wakimoto free field representation*, *Nuclear Physics B* **358** (1991) 547 – 570.
- [36] P. Christe and R. Flume, *The four-point correlations of all primary operators of the  $d = 2$  conformally invariant  $SU(2)\sigma$ -model with Wess-Zumino term*, *Nuclear Physics B* **282** (1987) 466 – 494.
- [37] G. Gori and J. Viti, *Four-point boundary connectivities in critical two-dimensional percolation from conformal invariance*, *Journal of High Energy Physics* **2018** (Dec, 2018) 131.